




Electron acoustic shock waves in nonisothermal dissipative plasmas

Arpita Shome^a , Sourav Pramanik, and Samiran Ghosh

Department of Applied Mathematics, University of Calcutta, 92, Acharya Prafulla Chandra Road, Kolkata 700009, India

Received 28 June 2022 / Accepted 1 November 2022 / Published online 16 November 2022
© The Author(s), under exclusive licence to EDP Sciences, SIF and Springer-Verlag GmbH Germany, part of Springer Nature 2022

Abstract. The propagation characteristics of weakly nonlinear electron acoustic waves in the presence of nonisothermal (trapped) hot electrons are investigated in collisional plasmas. The dynamics of the nonlinear waves are found to be governed by Schamel–Burgers and Schamel–Korteweg–de Vries–Burgers-type equations depending on the strength of the nonisothermal parameter. Burgers’ terms appear due to the anomalous dissipation introduced by the collisions between cold electrons and immobile ions in the presence of collective phenomena (plasma current). The derived nonlinear equations are solved analytically with the help of the *Tanh* method. The time-dependent computational results well agree with the analytical results and predict the possibility of the oscillatory and monotonic shock-like structures depending on the strength of the collisional drag and nonisothermality of hot electrons. The trapped electrons significantly modify the amplitude and width of the nonlinear pulse. The results may explain the shock formation and the particle acceleration mechanism in auroral plasma region.

1 Introduction

The electron acoustic waves (EAW) and its nonlinear characteristics have become an interesting topic of research because of its various applications in space [1–4] and laboratory plasmas [5–7]. This mode was first observed by Fried and Gould while solving the linear electrostatic Vlasov dispersion equation in an unmagnetized and homogeneous plasma [8]. From the dispersion relation, they identified the EAW mode along with the Langmuir and ion-acoustic waves in the presence of at least two species of electrons having higher and lower temperatures. Two-electron-temperature plasmas are frequently observed in the Earth’s bow shock planetary space [9, 10] and polar magnetosphere [2].

The EAW is a relatively low frequency ($kV_{Tc} \ll \omega \ll kV_{Th}$) wave [where $V_{Tc(h)} = \sqrt{T_{c(h)}/m}$ is the thermal velocity of the cold (hot) electron, $T_{c(h)}$ is the cold (hot) electron temperature and m is the mass of the electron] and its oscillation time scale $\sim \omega_{pc}^{-1}$ is much larger than that of hot electrons $\sim \omega_{ph}^{-1}$ (where $\omega_{pc(h)} = \sqrt{4\pi n_{c(h)0}e^2/m}$ is the cold (hot) electron plasma frequency and $n_{c(h)0}$ is the equilibrium number density of cold (hot) electrons). Thus for this wave mode, cold electrons provide the inertia to maintain the electrostatic oscillations and the restoring force comes from the hot electron pressure. To avoid the strong Landau damping for the existence of this mode, one

needs $T_c/T_h \lesssim 0.1$ and $n_{h0}/n_{c0} \gg 1$ [11]. The EAWs play a potential role in interpreting broadband electrostatic noise (BEN) noticed in various regions of the earth’s magnetosphere (detected by various satellites like Viking Fast) [8–10, 12–14] and also in geomagnetic tail [15].

EAW excitations are also found by the Fast Auroral Snapshot (FAST) observations in the intermediate-altitude (<4000 km) auroral region, [16] and by the POLAR observations [17] at higher auroral altitudes ($\sim 2R_E$, where R_E is the Earth radius). Interestingly, in the high-altitude POLAR observations, solitary structures have been detected in the regions of BEN in the presence of two-temperature electrons [18]. These waves are also identified experimentally in the presence of two types of electron species (hot and cold) [7]. In response to the relatively large amplitude disturbances, EAWs become nonlinear and exhibit different coherent nonlinear structures [19–24].

EAWs are often studied by considering the Maxwell–Boltzmann distributed hot electrons [12, 22–24]. However, various satellite and experimental observations reveal that the velocity distributions of the plasma particles deviate from the Maxwell–Boltzmann statistics due to the presence of nonisothermal particles [25–28]. Several studies on the nonlinear character of various acoustic modes have been performed incorporating non-Maxwellian electron distributions [29–32]. Schamel proposed a particular type of distribution function for the trapped (nonisothermal) particles which follow vortex-like distribution due to the formation of the phase

^a e-mail: arpitashome18@gmail.com (corresponding author)

space holes [33–37]. Effects of such trapped particles on the nonlinear EAWs have been inspected by a few authors [38, 39]. The trapping of electrons connected to the EAW excitation has also been noted in the laboratory during the interactions of plasma with laser and electron beams [40, 41]. Moreover, the FAST satellite observations imply that particle acceleration in auroral plasma is caused by the parallel electric field resulting from a monotonic potential ramp (double layer or shock-like) and the drift of the accelerated electrons across the ramp leads to the formation of electron phase-space holes [42–45]. Since the presence of two kinds of electrons (hot and cold) is fairly frequent in such regions [13, 16], these electrons may have significant effects on the development of shock-like structures and particle acceleration process.

Nonetheless, the collisions between plasma particles can affect the evolution of EAWs substantially. It serves an important role in plasma transport processes in laboratory and space domains (e.g., at the auroral ionosphere altitude collisional process is considerable) [46]. Usually, collisions between two different species give rise to the Korteweg–de Vries (KdV) equation with a linear damping term [47]. Moreover, these collisions under certain physical conditions can also introduce Burgers' term in the KdV equation that exhibits shock-like structures [22, 48]. Studies on the different kinds of nonlinear plasma waves have been reported in the presence of various dissipative sources [49–52]. The electron acoustic shock wave (EASW) has been studied recently in the presence of Maxwell–Boltzmann distributed hot electrons [22]. But the possibility of the shock structures in collisional plasmas has not been investigated yet in the presence of nonisothermal hot electrons. Thus it is instructive to investigate the effects of nonisothermal hot electrons on nonlinear coherent structures of EAWs in collisional plasmas.

This work aims to investigate the impacts of nonisothermal electrons on the one dimensional (1D) weakly nonlinear dynamics of EAWs in weak collisional plasmas under the assumption that the cold electron-stationary ion collisional frequency (ν_c) is smaller than the cold electron oscillation frequency (ω_{pc}). To incorporate the nonisothermality in the plasma, we follow the original works of Schamel [33–36] for hot electrons. The presence of nonisothermal electrons introduces two regimes of physical interests: weak [$b \sim O(\sqrt{\epsilon})$, b is the nonisothermal parameter and ϵ is a parameter that determines the amplitude of the perturbation] and strong [$b \gg O(\sqrt{\epsilon})$] [33–36]. The reductive perturbation technique (RPT) is used to study the weakly nonlinear dynamics which shows that in the cases of weak and strong nonisothermality, the EAW dynamics are governed by Schamel–Korteweg–de Vries–Burgers (SKdVB) and Schamel–Burgers (SB)- type equations, respectively. These two equations are solved analytically using ‘*Tanh method*’ [53]. The cold electron-ion collision is responsible for the Burgers' term which indicates the possibility of the shock-like structures of EAWs. The analytical and computational results pre-

dict the formation of electron acoustic shock structures due to collisions. The fixed point analysis reveals that in the case of weak nonisothermality the nonlinear EAW (governed by the SKdVB equation) exhibits only monotonic shock structures due to the presence of higher (two) nonlinear terms as confirmed by the time-dependent numerical investigations.

This paper is organized in the following manner. Section 2 contains the physical model and basic equations. The nonlinear evolution equations are derived in Sect. 3. Approximate analytical solutions are provided in Sect. 4. Comments on the linear stability through fixed point analysis are placed in Sect. 5. Particular type of shock solutions is found using the *Tanh* method in Sect. 6. The computational results and their graphical representations are discussed in Sect. 7. The results and their physical implications are briefly summarized in Sect. 8.

2 The model and basic equations

We consider an unbounded, homogeneous and unmagnetized plasma which is composed of immobile ions, cold and nonisothermal hot electrons. The ions are assumed to form stationary charge neutralizing background with uniform density (n_0). The charge neutrality condition is

$$n_{h0} + n_{c0} = n_0, \quad (1)$$

where $n_{c(h)0}$ denotes the equilibrium density of cold (hot) electrons.

In 1D the dynamics of cold electron is governed by the continuity equation,

$$\frac{\partial n_c}{\partial t} + \frac{\partial(n_c u_c)}{\partial x} = 0, \quad (2)$$

and the momentum equation,

$$m n_c \left(\frac{\partial u_c}{\partial t} + u_c \frac{\partial u_c}{\partial x} \right) = -n_c e E - m n_c \nu_c u_c, \quad (3)$$

where e is the magnitude of the electronic charge, n_c is the density of cold electrons, u_c is the cold electron fluid velocity along the x -direction, ν_c is the collision frequency between cold electrons and stationary background ions (large mass) and E is the electric field in the x -direction. All the variables are assumed to depend on single space coordinate x and time t . It is assumed that $T_c \ll T_h$, so we can neglect the pressure term in the momentum equation [Eq. (3)]. Also, the collisions between cold electrons and stationary ions give rise to a dissipative force $-m n_c \nu_c u_c$ in the right-hand side of momentum equation (3).

For closure of the plasma system, we consider the equations for E from Maxwell's equations,

$$\frac{\partial E}{\partial x} = 4\pi e(n_0 - n_c - n_h); \quad \frac{\partial E}{\partial t} = 4\pi en_c u_c. \quad (4)$$

Here n_h is the density of hot electrons. Since the EAWs are related to the parallel electric field (E_{\parallel}) fluctuations [11], $\nabla \times E = 0$. It implies that the mode is purely electrostatic and there is no inherent magnetic field so that $\nabla \times B = 0$. In such context, the displacement current ($\partial E/\partial t$) balances the particle current ($en_c u_c$) which is reflected by the second equation of Eq. (4). Furthermore, since hot electrons are Schamel distributed, they do not have directed resultant velocity to contribute to the current and therefore, the current is carried only by the cold electron species [54]. Using Eq. (4) with $E = -\partial\varphi/\partial x$ (φ is the electrostatic potential), Eq. (3) gives

$$\left(\frac{\partial}{\partial t} + u_c \frac{\partial}{\partial x}\right) u_c = \frac{e}{m} \frac{\partial \varphi}{\partial x} + \frac{\nu_c}{4\pi en_c} \frac{\partial}{\partial t} \left(\frac{\partial \varphi}{\partial x}\right). \quad (5)$$

To investigate the dynamics of nonlinear EAW, we consider the dimensionless variables as: $\hat{x} = x/\lambda_D$ (where $\lambda_D = \sqrt{T_h/4\pi n_{c0}e^2}$ is the plasma Debye length), $\hat{t} = \omega_{pc}t$, $\hat{n}_c = n_c/n_{c0}$, $\hat{n}_h = n_h/n_{h0}$, $\hat{\phi} = e\varphi/T_h$ and $\hat{u}_c = u_c/v_{th}$. Hereafter, we remove the notation hat from the variables for simplicity and work with the normalized variables. Thus in normalized forms, the continuity and momentum equations [Eqs. (2), (3)] can be expressed as

$$\frac{\partial n_c}{\partial t} + \frac{\partial(n_c u_c)}{\partial x} = 0, \quad (6)$$

$$\frac{\partial u_c}{\partial t} + u_c \frac{\partial u_c}{\partial x} = \frac{\partial \phi}{\partial x} + \frac{\bar{\nu}_c}{n_c} \frac{\partial}{\partial t} \left(\frac{\partial \phi}{\partial x}\right), \quad \bar{\nu}_c = \frac{\nu_c}{\omega_{pc}}. \quad (7)$$

The Poisson's equation [first equation in Eq. (4)] then becomes

$$\frac{\partial^2 \phi}{\partial x^2} = \frac{1}{\alpha} n_h + n_c - \left(\frac{n_0}{n_{c0}}\right), \quad \alpha = \frac{n_{c0}}{n_{h0}}. \quad (8)$$

Here $\alpha < 1$ as it is necessary condition for the existence of the EAW. Due to the nonisothermality of hot electrons, the density of hot electrons can be assumed as [34, 36]

$$n_h = 1 + \phi - b\phi^{3/2} + \frac{\phi^2}{2} + \dots, \quad b = \frac{4(1-\beta)}{3\sqrt{\pi}}, \quad (9)$$

$$\beta = \frac{T_h}{T_{ht}},$$

where T_{ht} is the temperature of the trapped hot electrons. The parameter β is a measure of the energy ratio of the free to trapped hot electrons, known as a trapping parameter, signifying a vortex distribution (hole in a

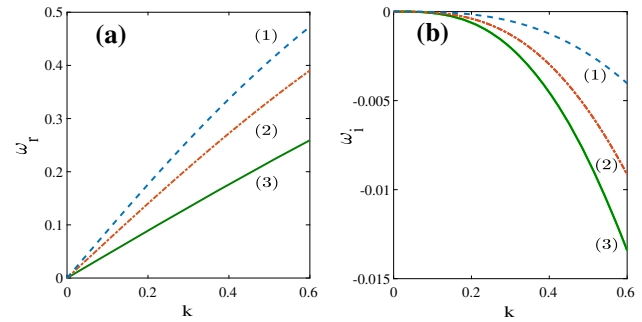


Fig. 1 Linear dispersion curves: Dependencies of **a** real (ω_r) and **b** imaginary (ω_i) parts of the frequency with wavenumber k for $\bar{\nu}_c = 0.2$. (1) Blue dashed curve ($\alpha = 0.2$), (2) Red dashed-dotted curve ($\alpha = 0.5$), (3) Green solid curve ($\alpha = 0.8$)

phase-space) for $\beta < 0$, a flat top distribution for $\beta = 0$ and Maxwellian distribution for $\beta = 1$ [34, 36]. Here, we are interested in both the regimes where b is relatively small ($\beta \in [0, 1]$) and large ($\beta < 0$), respectively. Physically, the large values of b for $\beta < 0$ indicate the large number of trapped electrons in the plasma system.

Linearizing the equations [Eqs. (6)–(8)] in a homogeneous background and assuming that all the perturbed variables vary as $\exp[i(kx - \omega t)]$, we derive the dispersion relation as

$$\omega^2 = \frac{\alpha k^2}{1 + \alpha k^2} - i \frac{\bar{\nu}_c \alpha \omega k^3}{1 + \alpha k^2}, \quad (10)$$

where $\omega (\equiv \omega/\omega_{pc})$ and $k (\equiv k\lambda_D)$ are normalized frequency and the wave number of the disturbances, respectively. In the presence of dissipation, we assume $\omega = \omega_r(k) + i\omega_i(k)$ (where ω_r and ω_i are the real and imaginary parts of ω , respectively with $|\omega_i| \ll |\omega_r|$) and obtain the roots of the dispersion relation (10) as

$$\omega_r = \pm \sqrt{\frac{\alpha k^2}{1 + \alpha k^2} - \omega_i^2}, \quad \omega_i = -\frac{\bar{\nu}_c \alpha k^3}{2(1 + \alpha k^2)}. \quad (11)$$

This clearly shows that the EAW is damped due to collisions. The variations of ω_r and ω_i with k are provided in Fig. 1. The curves in this figure show that the damping rate increases with the increase in α (cold to hot density ratio). In the proceeding sections, it will be shown that this dissipation provides weak shock structure in the nonlinear regime.

3 Derivation of nonlinear evolution equations

To derive the nonlinear transport equation for EAWs in the presence of nonisothermal electrons, we consider two physically relevant cases: the nonisothermal parameter b is (i) small and (ii) relatively large. Here to investigate the weakly nonlinear dynamics of EAW in collisional nonisothermal plasmas, we employ the RPT [55]

and introduce the following stretched coordinates;

$$\xi = \epsilon^p(x - \lambda t), \quad \tau = \epsilon^{3p}t. \tag{12}$$

where λ is the phase velocity of the EAW normalized in unit of V_{Th} and ϵ is the dimensionless (small but nonzero) parameter characterizing the strength of the nonlinearity. The dependent variables are expanded as

$$h = h_0 + \epsilon h_1 + \sum_{j=1}^{\infty} \epsilon^{2p+j} h_{j+1}, \tag{13}$$

where $h_0 = 1$ for $h = n_c$ and $h_0 = 0$ for $h = u_c$ and ϕ . To incorporate the weak ($\nu_c < \omega_{pc}$) collisional effects in the nonlinear regime, we consider the following consistent scaling:

$$\bar{\nu}_c = \frac{\nu_c}{\omega_{pc}} \sim \nu \epsilon^p. \tag{14}$$

The values of $p \in (0, 1)$ depend on the strength of the nonisothermal parameter b .

3.1 Weak nonisothermality ($b \sim O(\sqrt{\epsilon})$)

In this case of weak nonisothermality, we take $p = 1/2$. With this value of p , we substitute Eqs. (12), (13) and (14) into Eqs. (6)–(9) and the continuity, momentum and Poisson’s equations, respectively, become

$$\begin{aligned} &\epsilon^{3/2} \left[-\lambda \frac{\partial n_{c1}}{\partial \xi} + \frac{\partial u_{c1}}{\partial \xi} \right] + \epsilon^{5/2} \left[\frac{\partial n_{c1}}{\partial \tau} - \lambda \frac{\partial n_{c2}}{\partial \xi} \right. \\ &\quad \left. + \frac{\partial u_{c2}}{\partial \xi} + \frac{\partial(n_{c1}u_{c1})}{\partial \xi} \right] + \text{h.o.t} = 0, \\ &\epsilon^{3/2} \left[-\lambda \frac{\partial u_{c1}}{\partial \xi} - \frac{\partial \phi_1}{\partial \xi} \right] + \epsilon^{5/2} \left[\frac{\partial u_{c1}}{\partial \tau} + u_{c1} \frac{\partial u_{c1}}{\partial \xi} \right. \\ &\quad \left. - \lambda \frac{\partial u_{c2}}{\partial \xi} - \frac{\partial \phi_2}{\partial \xi} + \nu \lambda \frac{\partial^2 \phi_1}{\partial \xi^2} \right] + \text{h.o.t} = 0, \\ &\epsilon \left[\alpha n_{c1} + \phi_1 \right] + \epsilon^2 \left[\alpha \frac{\partial^2 \phi_1}{\partial \xi^2} - \phi_2 - \frac{\phi_1^2}{2} \right. \\ &\quad \left. + b \phi_1^{3/2} - \alpha n_{c2} \right] + \text{h.o.t} = 0. \end{aligned} \tag{15}$$

Here h.o.t. means higher-order terms. Collecting the coefficients of lowest powers of ϵ , we get

$$\alpha n_{c1} + \phi_1 = 0, \quad u_{c1} - \lambda n_{c1} = 0, \quad \lambda u_{c1} + \phi_1 = 0. \tag{16}$$

These equations self-consistently determine the phase velocity of the EAWs [11]:

$$\lambda^2 = \alpha \Rightarrow \omega/k = \sqrt{\frac{n_{c0} T_h}{n_{h0} m}} \quad (\text{dimensional form}). \tag{17}$$

In the next higher order of ϵ , we eliminate all the second order terms in Eq. (15) with the help of first order relations (16) and after some algebraic manipulations, we get the following SKdVB equation,

$$\frac{\partial \phi_1}{\partial \tau} - \alpha_2 \phi_1 \frac{\partial \phi_1}{\partial \xi} + \alpha_1 \sqrt{\phi_1} \frac{\partial \phi_1}{\partial \xi} + l \frac{\partial^3 \phi_1}{\partial \xi^3} = \mu \frac{\partial^2 \phi_1}{\partial \xi^2}, \tag{18}$$

where,

$$\alpha_2 = \frac{\sqrt{\alpha}}{2} \left(1 + \frac{3}{\alpha} \right), \quad \alpha_1 = \frac{3b \sqrt{\alpha}}{4}, \quad l = \frac{\alpha^{3/2}}{2}, \quad \mu = \frac{\alpha \nu}{2}. \tag{19}$$

Here the coefficient of the Burgers’ term μ ($\propto \nu$) arises due to the collision between cold electrons and stationary ions. In the above Eq. (18), if we put $b = 0$ ($\beta = 1$) to represent the Maxwellian hot electrons, we recover the KdVB equation for EAW [22].

3.2 Strong nonisothermality ($b \gg O(\sqrt{\epsilon})$)

In this case of strong nonisothermality, we take $p = 1/4$. With this value of p , proceeding as before, from the basic equations [Eqs. (6)–(9)] we obtain

$$\begin{aligned} &\epsilon^{3/2} \left[-\lambda \frac{\partial n_{c1}}{\partial \xi} + \frac{\partial u_{c1}}{\partial \xi} \right] + \epsilon^{5/2} \left[\frac{\partial n_{c1}}{\partial \tau} - \lambda \frac{\partial n_{c2}}{\partial \xi} \right. \\ &\quad \left. + \frac{\partial u_{c2}}{\partial \xi} \right] + \text{h.o.t} = 0, \\ &\epsilon^{3/2} \left[-\lambda \frac{\partial u_{c1}}{\partial \xi} - \frac{\partial \phi_1}{\partial \xi} \right] + \epsilon^{5/2} \left[\frac{\partial u_{c1}}{\partial \tau} - \lambda \frac{\partial u_{c2}}{\partial \xi} \right. \\ &\quad \left. - \frac{\partial \phi_2}{\partial \xi} + \nu \lambda \frac{\partial^2 \phi_1}{\partial \xi^2} \right] + \text{h.o.t} = 0, \\ &\epsilon \left[\alpha n_{c1} + \phi_1 \right] + \epsilon^2 \left[\alpha \frac{\partial^2 \phi_1}{\partial \xi^2} - \phi_2 + b \phi_1^{3/2} \right. \\ &\quad \left. - \alpha n_{c2} \right] + \text{h.o.t} = 0. \end{aligned} \tag{20}$$

The lowest order of ϵ gives the same set of equations [Eq. (16)], which determines the value of λ given in Eq. (17). Once again we eliminate all the second order terms from equations (20) for next leading order to obtain the following SB equation for finite amplitude nonlinear

EAWs in collisional nonisothermal plasmas;

$$\frac{\partial \phi_1}{\partial \tau} + \alpha_1 \sqrt{\phi_1} \frac{\partial \phi_1}{\partial \xi} + l \frac{\partial^3 \phi_1}{\partial \xi^3} = \mu \frac{\partial^2 \phi_1}{\partial \xi^2}. \tag{21}$$

4 Approximate solitary wave solution: decay of a solitary wave

Here we derive the stationary frame analytical solutions of Eqs. (18) and (21). To do this, we introduce the stationary frame $\chi = u_f \tau - \xi$, where u_f is the frame velocity related to the Mach number M by the general relation [using Eq. (12)]

$$M = 1 + \epsilon^{2p} \frac{\tilde{u}_f}{c_s}, \tag{22}$$

where \tilde{u}_f is the unnormalized frame velocity and $c_s = (\alpha T_h/m)^{1/2}$ is the EAW speed. Here $p = 1/2$ and $1/4$, respectively, for Eqs. (18) and (21).

It is well known that in the absence of collision $\mu = 0$ ($\nu_c = 0$), Eq. (18) reduces to the following SKdV equation [33]

$$\frac{\partial \phi_1}{\partial \tau} - \alpha_2 \phi_1 \frac{\partial \phi_1}{\partial \xi} + \alpha_1 \sqrt{\phi_1} \frac{\partial \phi_1}{\partial \xi} + l \frac{\partial^3 \phi_1}{\partial \xi^3} = 0, \tag{23}$$

which is exactly integrable and possesses the solitary wave solution [33]

$$\phi_1 = \Psi \frac{\text{sech}^4(w\chi)}{[1 - \delta \tanh^2(w\chi)]^2}, \quad w = \frac{1}{4} \sqrt{\frac{u_f}{l}} = \frac{1}{4} \sqrt{\frac{2u_f}{\alpha^{3/2}}}, \tag{24}$$

where w is the inverse of the width of the solitary wave. The amplitude Ψ and the parameter δ are given by

$$\Psi = \left[\frac{15u_f}{4\alpha_1(1 + \sqrt{\Delta})} \right]^2, \quad \delta = \frac{16\alpha_1^2(1 - \sqrt{\Delta})^2}{75\alpha_2 u_f}, \quad \Delta = 1 - \Delta_c, \tag{25}$$

where $\Delta_c = 75\alpha_2 u_f / (16\alpha_1^2)$. It is to be noted that for the real solution, we must have

$$1 < \Delta_c \Rightarrow u_f < \frac{16\alpha_1^2}{75\alpha_2} \Rightarrow M < 1 + \frac{6\epsilon b^2}{25} \left(\frac{\alpha^{3/2}}{3 + \alpha} \right), \tag{26}$$

so that the EA solitary wave propagate with a restricted speed.

Moreover, in the absence of α_2 ($\alpha_2 = 0 = \delta$), Eq. (21) reduces to the following Schamel equation [33]

$$\frac{\partial \phi_1}{\partial \tau} + \alpha_1 \sqrt{\phi_1} \frac{\partial \phi_1}{\partial \xi} + l \frac{\partial^3 \phi_1}{\partial \xi^3} = 0 \tag{27}$$

and the solitary wave solution of this equation is recovered in the limit $\alpha_2 \rightarrow 0$ ($\delta \rightarrow 0$) as

$$\phi_1 = \Psi_s \text{sech}^4(w\chi), \quad \Psi_s = \frac{1}{4} \left(\frac{15u_f}{4\alpha_1} \right)^2. \tag{28}$$

Interestingly, in this case there is no restriction on u_f and the EA solitary waves propagate with arbitrary speed.

In the presence of the dissipation ($\mu \neq 0$), the wave energy of both the equations [Eqs. (18) and (21)]

$$\frac{1}{2} \frac{\partial}{\partial \tau} \int_{-\infty}^{\infty} \phi_1^2 d\xi = -\mu \int_{-\infty}^{\infty} \left(\frac{\partial \phi_1}{\partial \xi} \right)^2 d\xi \tag{29}$$

is not conserved, and thereby, Eqs. (18) and (21) are not exactly integrable. However, we can derive an approximated analytical solution in the presence of weak dissipation ($\mu \ll 1$) using perturbation method [56, 57] and assume that the solitary wave amplitude, velocity and also the width of the solitary wave is slowly varying function of time (τ).

First we consider the SKdVB equation [Eq. (18)] and assume the solitary wave solution of the form

$$\phi_1 = \Psi(\tau) \frac{\text{sech}^4\{w(\tau)(\int_0^\tau u_f(\tau') d\tau' - \xi)\}}{[1 - \delta \tanh^2\{w(\tau)(\int_0^\tau u_f(\tau') d\tau' - \xi)\}]^2}. \tag{30}$$

Substituting this solution in the energy conservation Eq. (29), we obtain the following differential equation;

$$\frac{dg(\tau)}{d\tau} = -\mu s(\tau), \tag{31}$$

where the functions $g(\tau)$ and $s(\tau)$ are given by

$$g(\tau) = \frac{\Psi^2(\tau)}{w(\tau)} \left(\frac{16}{35} + \frac{64\delta}{315} \right), \quad s(\tau) = w(\tau) \Psi^2(\tau) (1 - \delta)^2 \left(\frac{512}{315} + \frac{1024\delta}{385} \right). \tag{32}$$

Unfortunately the differential equation (31) is too rigorous to solve analytically. Numerical solution of this equation provided in Fig. 2a, shows that the nonlinear wave amplitude decreases with time because of the dissipative factor μ ($\propto \nu$). To illustrate this phenomenon more precisely, we represent the solution [Eq. (30)] for $\mu = 0.2$ graphically in Fig. 2c which clearly show the decay of the solitary wave amplitude with time.

Next we consider the SB equation [Eq. (21)]. We have already seen that in the absence of dissipation, the solution of this equation is obtained by substituting $\alpha_2 = 0$ ($\delta = 0$) in the solution of SKdV equation [see Eqs. (24) and (28)] and thereby the energy equation (31) for the SB equation can be written as [putting $\delta = 0$ in Eq. (32)]

$$\frac{d\Psi_s(\tau)}{d\tau} = -\Upsilon \Psi_s^{3/2}(\tau), \quad \Upsilon = \frac{16\nu b}{315}. \tag{33}$$

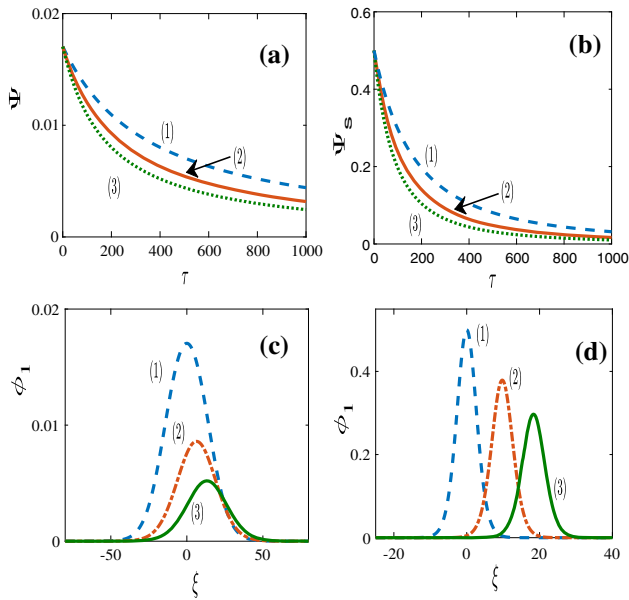


Fig. 2 **a, b** Variations of soliton amplitudes $\psi(\tau)$ with time τ . **c, d** Time evolution of soliton profiles $\phi_1(\tau)$ for $\nu = 0.2$. **a** and **c** $b \sim O(\sqrt{\epsilon})$, $\beta = 0.15$, $\alpha = 0.9$. **b** and **d** $b > O(\sqrt{\epsilon})$, $\beta = -0.1$, $\alpha = 0.8$. **a** and **b** (1) Blue dashed curve ($\nu = 0.2$), (2) Red solid curve ($\nu = 0.3$), (3) Green dotted curve ($\nu = 0.4$). **c**: (1) Blue dashed curve ($\tau = 0$), (2) Red dashed-dotted curve ($\tau = 350$), (3) Green solid curve ($\tau = 800$). **d** (1) Blue dashed curve ($\tau = 0$), (2) Red dashed-dotted curve ($\tau = 50$), (3) Green solid curve ($\tau = 100$)

The solution of this equation is obtained as

$$\Psi_s(\tau) = \Psi_0 \left(1 + \frac{\Upsilon\sqrt{\Psi_0}}{2}\tau \right)^{-2}, \tag{34}$$

where Ψ_0 is the initial value of Ψ_s . This solution clearly shows that the nonlinear wave amplitude decays algebraically with time τ and decay rate increases with the increase in nonisothermality parameter b and collision (see Fig. 2b). The solitary profiles presented in Fig. 2d agree with our result.

5 Linear stability analysis: fixed point analysis

In this section, we present a fixed point analysis to study the linear stability of these two equations in the χ frame. Here, we first consider the SKdVB equation [Eq. (18); $b \sim O(\sqrt{\epsilon})$] which in the χ frame transform to the following ordinary differential equation

$$-u_f \frac{d\phi_1}{d\chi} + \alpha_1 \sqrt{\phi_1} \frac{d\phi_1}{d\chi} - \alpha_2 \phi_1 \frac{d\phi_1}{d\chi} + l \frac{d^3\phi_1}{d\chi^3} + \mu \frac{d^2\phi_1}{d\chi^2} = 0. \tag{35}$$

The above equation after single integration (using the boundary conditions $\phi_1 \rightarrow 0; \frac{d\phi_1}{d\chi} \rightarrow 0; \frac{d^2\phi_1}{d\chi^2} \rightarrow 0$ as $|\chi| \rightarrow \infty$) becomes as follows:

$$\frac{d^2\phi_1}{d\chi^2} = \frac{2u_f}{\alpha\sqrt{\alpha}}\phi_1 - \frac{b}{\alpha}\phi_1^{3/2} + \frac{(1+\frac{3}{\alpha})}{2\alpha}\phi_1^2 - \frac{\nu}{\sqrt{\alpha}} \frac{d\phi_1}{d\chi}. \tag{36}$$

According to the theory of ordinary differential equation, this Eq. (36) has two fixed points: $(0, 0)$ and $(\phi^*, 0)$, where $\phi^{*2} = \phi_1$. The second fixed point ϕ^* is obtained from the relation

$$\frac{2u_f}{\alpha\sqrt{\alpha}} - \frac{b}{\alpha}\phi^* + \frac{(1+\frac{3}{\alpha})}{2\alpha}\phi^{*2} = 0. \tag{37}$$

This relation yields

$$\phi^* = \phi_{\pm}^* = \left(1 + \frac{3}{\alpha} \right)^{-1} \left[b \pm \sqrt{b^2 - \frac{4u_f(1+\frac{3}{\alpha})}{\sqrt{\alpha}}} \right]. \tag{38}$$

Using Eq. (22) [with $p = 1/2$], the reality condition of the solution yields

$$u_f < \frac{b^2\alpha^{3/2}}{4(\alpha+3)} \Rightarrow M < 1 + \frac{\epsilon b^2}{4} \left(\frac{\alpha}{3+\alpha} \right). \tag{39}$$

This fixed point is always positive. However, for Maxwellian distributed hot electrons ($b = 0$), Eq. (38) shows that second fixed point ($\phi_1 = \phi^{*2}$) is always negative [22]. Also using the reality condition [Eq. (39)] and expanding Eq. (38) binomially, we obtain

$$\phi_+^* \approx 2b \left(1 + \frac{3}{\alpha} \right)^{-1}, \quad \phi_-^* \approx \frac{2u_f}{b\sqrt{\alpha}}. \tag{40}$$

To study the nature of the fixed points $(0, 0)$ and $(\phi^*, 0)$, we linearize Eq.(36) (assuming that the dynamical variables $\sim \exp(\Lambda\chi)$, Λ is the eigenvalue) [58] about these fixed points and determine the corresponding eigenvalues. The eigenvalues corresponding to $(0, 0)$ are given by

$$\Lambda_{(0,0)} = \frac{1}{2\sqrt{\alpha}} \left[-\nu \pm \sqrt{\nu^2 + \frac{8u_f}{\sqrt{\alpha}}} \right] = \frac{1}{2\sqrt{\epsilon\alpha}} \left[-\bar{\nu}_c \pm \sqrt{\bar{\nu}_c^2 + 8(M-1)} \right]. \tag{41}$$

This clearly shows that the fixed point $(0, 0)$ is a saddle point as $M > 1$ [Eq. (22) with $p = 1/2$]. The eigenvalues corresponding to $(\phi^*, 0)$ are given by

$$\Lambda_{(\phi^*,0)} = \frac{1}{2\sqrt{\alpha}} \left[-\nu \pm \sqrt{\nu^2 - \frac{8u_f}{\sqrt{\alpha}} + 2b\phi^*} \right]. \tag{42}$$

The stability criteria of the fixed point $(\phi^*, 0)$ at the upstream side $(\chi \rightarrow -\infty)$ require

$$A_{(\phi^*, 0)} > 0 \Rightarrow b\phi^* < \frac{4u_f}{\sqrt{\alpha}}. \tag{43}$$

One can easily observe that the approximated value of ϕ_+^* root [Eq. (40)] does not satisfy this stability criteria due to the reality condition [Eq. (39)]. However, the stability condition is obvious for the ϕ_-^* root. Thus the fixed point $(\phi_-^*, 0)$ is a stable node and we get only the monotonic shock-like structures as the stable node corresponds to the monotonic shock. Interestingly for the Maxwellian case ($b = 0$) such restriction does not appear [22]. The strength of the shock is given as [58] $\phi_1(-\infty) - \phi_1(\infty) = \phi_-^{*2}$.

Next we consider the SB equation [Eq. (21); $b \gg O(\sqrt{\epsilon})$], which in the χ frame transform to the following ordinary nonlinear differential equation,

$$-u_f \frac{d\phi_1}{d\chi} + \alpha_1 \sqrt{\phi_1} \frac{d\phi_1}{d\chi} + l \frac{d^3\phi_1}{d\chi^3} + \mu \frac{d^2\phi_1}{d\chi^2} = 0. \tag{44}$$

After single integration (with localized boundary conditions), above equation becomes

$$\frac{d^2\phi_1}{d\chi^2} = \frac{2u_f}{\alpha\sqrt{\alpha}}\phi_1 - \frac{b}{\alpha}\phi_1^{3/2} - \frac{\nu}{\sqrt{\alpha}} \frac{d\phi_1}{d\chi}. \tag{45}$$

As before, this equation has two fixed points $(0, 0)$ and $(\phi^{*2}, 0)$, where

$$\phi^* = \frac{2u_f}{b\sqrt{\alpha}} = \frac{2(M-1)}{b\sqrt{\epsilon}}. \tag{46}$$

The corresponding eigenvalues are, respectively,

$$A_{(0,0)} = \frac{1}{2\sqrt{\alpha\sqrt{\epsilon}}} \left[-\bar{\nu}_c \pm \sqrt{\bar{\nu}_c^2 + 8(M-1)} \right], \tag{47}$$

$$A_{(\phi^*,0)} = \frac{1}{2\sqrt{\alpha\sqrt{\epsilon}}} \left[-\bar{\nu}_c \pm \sqrt{\bar{\nu}_c^2 - 4(M-1)} \right]. \tag{48}$$

These clearly reveal that the fixed point $(0, 0)$ is a saddle point [$M > 1$ according to Eq. (22) with $p = 1/4$], whereas the fixed point $(\phi^{*2}, 0)$ is a stable focus or stable node according as

$$1 + \frac{\bar{\nu}_c^2}{4} \leq M. \tag{49}$$

In case of stable focus (node), the solution provides an oscillatory (monotonic) shock-like structures and the strength of the shock is given as [58] $\phi_1(-\infty) - \phi_1(\infty) = 4u_f^2/(\alpha b^2)$. The trajectories and phase-space dynamics of a small disturbance around these fixed points are shown graphically in Fig. 3a–d, which validate the existence of shock solutions [60].

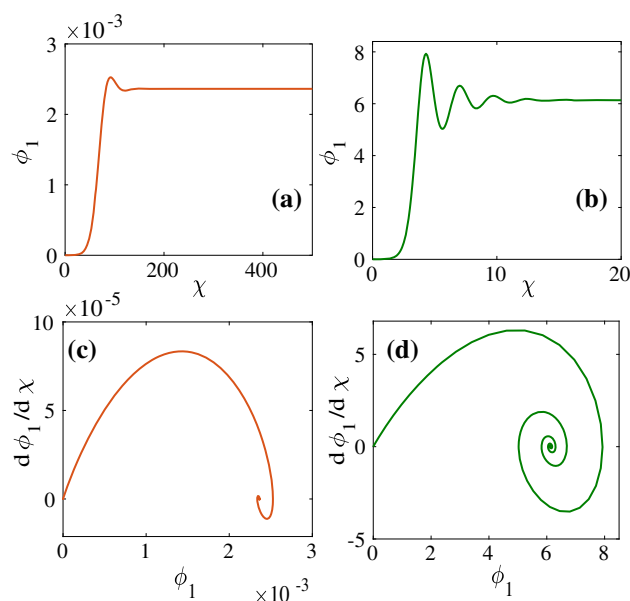


Fig. 3 Shock-like structure formation (a), (b) due to transition from unstable to stable fixed points and corresponding phase-portraits (c), (d). a, c $b \approx \sqrt{\epsilon}$ with $\beta = 0.1$, $\alpha = 0.6$, $\nu = 0.1$, $u_f = 0.01$, b, d $b \gg \sqrt{\epsilon}$ with $\beta = -0.2$, $\alpha = 0.2$, $\nu = 0.4$, $u_f = 0.5$

6 Particular type of shock solutions

In the previous sections, we have seen that the derived SB and SKdVB equations [Eqs. (18) and (21)] are not exactly solvable in the presence of Burgers’ term due to collision. However, the linear stability analysis predicts the possibility of shock solutions of both the equations [Eqs. (18) and (21)]. Thus in this section, one can find a particular type of analytical shock solutions of these equations by employing the well-known *Tanh method* [53]. Accordingly, we introduce a stationary wave profile $\phi_1(\xi, \tau) = \phi_1(\chi)$ and transform these equations [Eqs. (18) and (21)] in the wave frame χ . First we have taken Eq. (18) which corresponds to Eq. (35) in the χ frame and following the standard procedure [53], the particular analytical solution of Eq. (18) can be obtained as (see “Appendix”)

$$\phi_1(\xi, \tau) = \frac{\Phi}{4} [1 - \tanh(c(u_f\tau - \xi))]^2. \tag{50}$$

The expressions for Φ , and c are given by,

$$\begin{aligned} \Phi &= \left(1 + \frac{3}{\alpha}\right)^{-2} \left[b - \sqrt{b^2 - \frac{4u_f(1 + \frac{3}{\alpha})}{\sqrt{\alpha}}} \right]^2; \\ c &= \frac{1}{10} \left[\sqrt{\frac{3b^2}{\alpha + 3}} + \frac{\nu}{\sqrt{\alpha}} \right]. \end{aligned} \tag{51}$$

In the absence of trapped electrons ($b = 0 \Rightarrow \alpha_1 = 0$), Eq.(18) reduces to the well known KdV-Burgers equation [58] and its particular type of analytical solution can be easily be recovered from our solution given in Eq.(51) by

putting $b = 0$ {similar to the solutions (14) and (15) in Ref. [53]}. Also the value of the amplitude Φ is consistent with our fixed point ϕ_{-}^{*2} [Eq. (38)].

Next, we consider SB equation [Eq. (21); $b \gg O(\sqrt{\epsilon})$] which in the χ frame transform to Eq. (44). Proceeding as before the particular analytical solution of Eq. (21) can be obtained as (see ‘‘Appendix’’)

$$\phi_1(\chi) = \Phi_s \left[\frac{1 - \tanh(c\chi)}{2} \right]^4, \tag{52}$$

where

$$\Phi_s = \left(\frac{2u_f}{b\sqrt{\alpha}} \right)^2, \quad c = \frac{\nu}{18\sqrt{\alpha}}. \tag{53}$$

This value of Φ_s is also consistent with the fixed point ϕ^{*2} [Eq. (46)].

7 Computational results

To demonstrate the nature of the shock-structures, in this section, we solve SKdVB [Eq. (18)] and SB [Eq. (21)] equations numerically using the finite difference scheme and the results are shown graphically in Figs. 4 and 5. For this purpose, we consider the following step-like wave form as initial input [22]

$$\phi(\xi, 0) = \begin{cases} A & \text{if } \xi < 0 \\ \frac{A}{2} (1 + \cos(k\xi)) & \text{if } 0 < \xi < \pi/k \\ 0 & \text{if } \xi > \pi/k. \end{cases} \tag{54}$$

Here, A and k are the initial amplitude and wave number, respectively. The value of k determines the temporal evolution for fixed value of A . Eqs. (18) and (21) are solved within $[-L, L]$ with the above initial condition and the boundary conditions: $\phi(-L, \tau) = A$, $\phi(L, \tau) = 0$ and $\phi_\xi(-L, \tau) = 0 = \phi_\xi(L, \tau)$. In our computation we have set $L = 60, A = 0.1$ and $k = \pi/20$, with the density ratio $\alpha = 0.2$.

We investigate two different cases separately. In case of $b \approx O(\sqrt{\epsilon})$, only monotonic shock is observed from Eq. (18) irrespective of any ν values (see Fig. 4a, b) which well agree with the results of fixed point analysis in the previous section. It is to be noted that in case of Maxwellian hot electrons ($b = 0$), one can recover the previous results [22] using same initial conditions (54) except A is negative (as discussed in Sect. 5.) (also see Fig. 4c, d). Here the observed electron acoustic shocks are rarefaction shocks as $\phi_1 > 0 \Rightarrow n_{c1} < 0$ [see Eq. (16)].

On the other hand, for $b \gg O(\sqrt{\epsilon})$, we observe the oscillatory and monotonic shocks for the weak dissipation ($\nu = 0.1$) and the strong dissipation ($\nu = 1$), respectively. In Fig. 5, we present the development of shock structures at evolved times, corresponding to Eq. (21). In the upper panel, Fig. 5a, b displays the evolution of initial profile as oscillatory shocks for weak dissipation, respectively, for $\beta = -0.3$ and $\beta = -0.1$. However, Fig. 5c [$\beta = -0.3$] and d [$\beta = -0.1$]

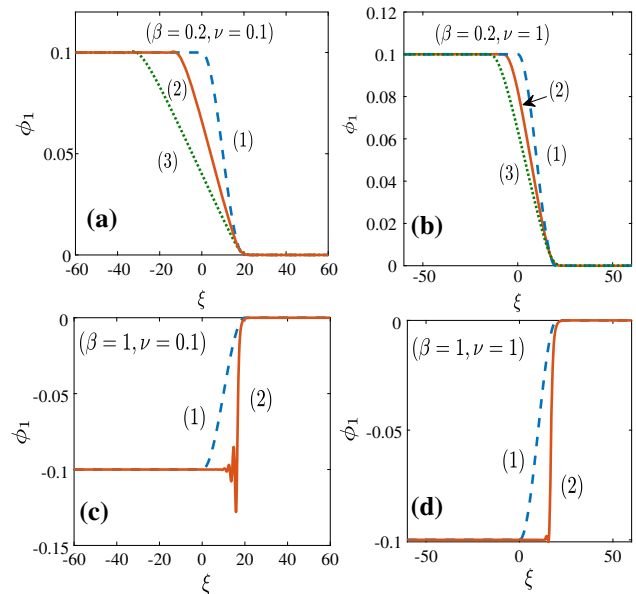


Fig. 4 Numerical solution of Eq. (18) for $\alpha = 0.2$. Blue dashed curves (1) in all figures correspond to initial profile at $\tau = 0$. Upper panel: Nonisothermal case for $\beta = 0.2$ (a), (b). **a** Monotonic shock structure for $\nu = 0.1$ and **b** $\nu = 1$. Curve (1): $\tau = 0$ [blue dashed], Curve (2): $\tau = 15$ [solid red], Curve (3): $\tau = 30$ [dotted green]. Lower panel: Maxwellian case with $\beta = 1$ (c), (d). **c** Oscillatory shock structure for $\nu = 0.1$ and $\tau = 20$ [Red solid Curve (2)]. **d** Monotonic shock structure for $\nu = 1$ and $\tau = 20$ [Red solid Curve (2)]

of lower panel shows the development of monotonic shock for stronger dissipation. The transition from the upstream to the far downstream state changes from a oscillatory to monotonic nature, as the magnitude of the dissipation coefficient ν increases. Thus our numerical investigations confirm the existence of shock-like structures in both cases.

It is to be noted that for the Burgers-type equations shock amplitude (shock strength) remains unaffected by dissipation while shock width gets modified by it [58,60]. Accordingly, with the increase in dissipation the shock becomes steep and the oscillatory to monotonic shock transition occurs [58,60]. The fixed point analysis, analytical solutions and also the computational results confirm these physical phenomena.

8 Discussions

In the present work, we have shown that the dissipation due to the collisions between the electron-stationary ion through the collective phenomena (plasma current) causes the EA shock structures in plasmas in the presence of nonisothermal hot electrons. This collisional dissipation leads to the Burgers’ term in the nonlinear evolution equation, which is responsible for the shock and plays a similar role as viscosity. Depending on the strength of the nonisothermality, the transport phenomena of nonlinear EAW is described through the SKdVB and SB equations [Eqs. (18) and (21)]. The approximate analytic solutions of these equations show

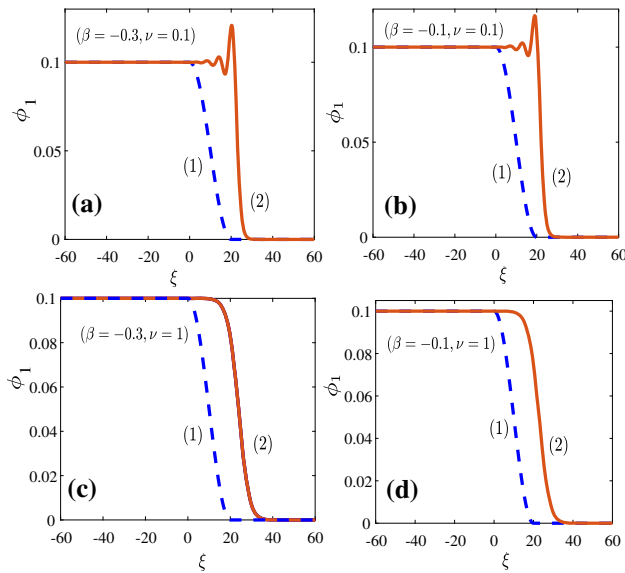


Fig. 5 Numerical solution of Eq. (21) for $\alpha = 0.2$. Blue dashed curves (1) in all figures correspond to initial profile at $\tau = 0$. Upper panel (a), (b) Oscillatory shock structures for weak collisional effect ($\nu = 0.1$) a Oscillatory shock for $\beta = -0.3$ at $\tau = 200$ [red solid curve (2)], b oscillatory shock for $\beta = -0.1$ at $\tau = 230$ [red solid curve (2)]. Lower panel (c), (d) Monotonic shock structures for stronger collisional effect ($\nu = 1$) c Monotonic shock for $\beta = -0.3$ at $\tau = 200$ [red solid curve (2)], b monotonic shock for $\beta = -0.1$ at $\tau = 230$ [red solid curve (2)]

that an initial solitary wave structure decays with time as shown in Eqs. (31) and (34) (also see Fig. 2). Physically, this decay is associated with development of a noise tail in consequence of soliton mass conservation and finally forms shock structures [56]. Because of this fact, the evolution equations are also solved analytically using ‘*Tanh method*’.

The time-dependent numerical and fixed point analysis of the SKdVB equation [Eq. (18)] reveal only the monotonic shock structures of nonlinear EAWs irrespective of the values of collision frequency (ν), whereas the SB equation [Eq. (21)] demonstrates both the oscillatory and monotonic shock structures depending on the values of ν . In contrast to the Maxwell–Boltzmann distributed hot electrons (see Ref. [22] where shocks are compression shocks), in the presence of nonisothermal hot electrons, the shocks are found to be rarefaction shocks in our work (see Figs. 4, 5).

The existence of EAWs and electrostatic shock-like structures in the presence of hot and cold electron populations have been observed in the auroral ionosphere and polar magnetosphere [1, 2, 13, 42]. Therefore, the results of the present investigation could be useful to qualitatively explain the origin of shock waves in such regions. Satellite observations confirm that the double layers or shock-like coherent structures self consistently generate $E_{||}$ which is responsible for the particle acceleration in auroral plasmas [42–45]. Furthermore, hot electrons often get trapped in the wave potential and follow a vortex-like nonisothermal distribution (non-Maxwellian) due to the formation of phase space holes [33]. These trapped electrons (nonisothermal) play a crucial role to govern the spatial distribution of the auroral potential

[44]. The results of the present investigation could be useful for the understanding the physics of shock wave in the auroral plasma region. Moreover, the electrons are energized due to the passing of the shock wave, which initiates the particle acceleration mechanism in the auroral region. Thus the results presented here could be a viable physical process for the shock wave and particle acceleration in the auroral region.

The analytical solutions of both the equations [SKdVB Eq. (18) and SB Eq. (21)] show that the peak value of $E_{||} \sim \Phi(\Phi_s)c$. The plasma parameters in the auroral region are [13]: $n_{c0} \sim 0.5 \text{ cm}^{-3}$, $n_{h0} \sim 2.5 \text{ cm}^{-3}$ and $T_h \sim 250 \text{ eV}$, implying $\lambda_D \sim 166 \text{ m}$. For $\alpha = 0.4$ and $\nu = 0.4$ values, the solution [Eq. (51)] of the SKdVB equation with $\beta = 0.7$ ($b \sim 0.2$) and $u_f = 0.02$ estimates $c^{-1} \sim 12$ and $E_{||} \sim 2 \text{ mV/m}$, whereas the solution [Eq. (53)] of the SB equation with $\beta = -0.1$ ($b \sim 0.8$) and $u_f = 0.4$ estimates $c^{-1} \sim 28$ and $E_{||} \sim 123 \text{ mV/m}$. These peak values of $E_{||}$ well agree with the observed values by the Viking satellite [12]. This $E_{||}$ field generates a strong current across the potential ramp due to the drifting of accelerated electrons and a strong current can self consistently generate a magnetic field. The effects of the electron drift and also the magnetic field on nonlinear EAWs in the presence of trapped hot electrons are our future interest of investigation.

Acknowledgements The authors (A. S. and S. P.) would like to thank the DST and UGC, Govt. of India for providing INSPIRE Fellowship (Ref. DST/INSPIRE Fellowship/2017/IF170322) and Dr. D. S. Kothari Post Doctoral Fellowship(Ref. PH/19-20/0016), respectively. The authors thank the referees for the careful reading and offering constructive suggestions to improve the manuscript. The authors would also like to acknowledge Mr. Debkumar Chakraborty for his valuable help and suggestions.

Author contributions

All authors have contributed equally to the paper.

Data Availability Statement This manuscript has associated data in a data repository. [Authors’ comment: The data that support the findings of this study are available from the corresponding author upon reasonable request.]

Declarations

Conflict of interest The authors have no relevant financial or non-financial interests to disclose.

Appendix A: Derivations of the analytical shock solutions

In Eq. (35), we put $\phi_1(\chi) = f_1^2(Y)$ [where $Y = \tanh(c\chi)$ and c^{-1} is the characteristic width of the solution] to eliminate the square root term and substituting this, we obtain

$$\begin{aligned} &\mu c \left[(1 - Y^2) \frac{d}{dY} \left[2(1 - Y^2) f_1 \frac{df_1}{dY} \right] \right] \\ &= 2(u_f - \alpha_1 f_1 + \alpha_2 f_1^2) (1 - Y^2) f_1 \frac{df_1}{dY} \\ &\quad + lc^2(1 - Y^2) \frac{d}{dY} \left[(1 - Y^2) \frac{d}{dY} \left[2(1 - Y^2) f_1 \frac{df_1}{dY} \right] \right]. \end{aligned} \tag{A.1}$$

Following the standard procedure [53], $f_1(Y)$ is expressed as the power series of Y as

$$f_1(Y) = \sum_{n=0}^N a_n Y^n. \tag{A.2}$$

Substituting this expansion in (A.1) and then balancing the highest powers (the second and fourth terms in right-hand side), we obtain $N = 1$. Finally, we assume the solution of Eq. (35) of the form

$$\phi_1(\chi) = \Phi \left[\frac{1 - \tanh(c\chi)}{2} \right]^2. \tag{A.3}$$

Putting this solution into the ODE [Eq. (35)] and equating the coefficients of like powers of $\tanh(c\chi)$, we obtain the system of simultaneous homogeneous equations as

$$\begin{bmatrix} 1 & 2 & 1 & -1 & 1 \\ 1 & 8 & -2 & -2 & 3 \\ 1 & 8 & 4 & 0 & -2 \\ 1 & 20 & -2 & -2 & 2 \\ 0 & 6 & 3 & 1 & -3 \\ 0 & -12 & 0 & 0 & 1 \end{bmatrix} \begin{bmatrix} u_f \\ lc^2 \\ \mu c \\ \frac{\sqrt{\Phi}}{2\alpha_1} \\ \frac{\Phi}{4\alpha_2} \end{bmatrix} = \begin{bmatrix} 0 \\ 0 \\ 0 \\ 0 \\ 0 \\ 0 \end{bmatrix}. \tag{A.4}$$

After some elementary matrix operations, we obtain the following system of equations

$$\begin{aligned} u_f &= \frac{2\sqrt{\Phi}\alpha_1}{3} - \frac{\Phi\alpha_2}{2}, \quad lc^2 = \frac{\Phi\alpha_2}{48}, \\ \mu c &= -\frac{\sqrt{\Phi}\alpha_1}{6} + \frac{5}{24}\Phi\alpha_2. \end{aligned} \tag{A.5}$$

The last two equations are independent of u_f , and therefore, solving the first equation, we obtain

$$\sqrt{\Phi}_{\pm} = \frac{2\alpha_1}{3\alpha_2} \pm \sqrt{\left(\frac{2\alpha_1}{3\alpha_2}\right)^2 - \frac{2u_f}{\alpha_2}}. \tag{A.6}$$

However, only the Φ_- root yields the physically consistent solution (see Sect. 5) and thereby we consider only the root Φ_- as

$$\sqrt{\Phi} = \left(1 + \frac{3}{\alpha}\right)^{-1} \left[b - \sqrt{b^2 - \frac{4u_f(1 + \frac{3}{\alpha})}{\sqrt{\alpha}}} \right]. \tag{A.7}$$

This result well agree with our fixed point analysis of the SKdVB equation Eq.(18). Finally, the last two equations of Eq. (A.5) yields

$$c = \frac{\mu}{10l} \pm \frac{\alpha_1}{\sqrt{75\alpha_2 l}}. \tag{A.8}$$

This clearly shows in case of $-$ sign, the c^{-1} (width) becomes infinite at a critical value of μ , which is unphysical, and therefore, we consider

$$c = \left[\frac{\alpha_1}{\sqrt{75\alpha_2 l}} + \frac{\mu}{10l} \right] = \frac{1}{10} \left[\sqrt{\frac{3b^2}{\alpha + 3}} + \frac{\nu}{\sqrt{\alpha}} \right]. \tag{A.9}$$

Similarly, for SB equation [Eq. (21); $b \gg O(\sqrt{\epsilon})$], proceeding as before, we determine $N = 2$ and the solution is then assumed as

$$\phi_1(\chi) = \Phi_s \left[\frac{1 - \tanh(c\chi)}{2} \right]^4, \tag{A.10}$$

Substituting Eq. (A.10) into Eq. (44) and then equating the coefficients of different powers of $\tanh(c\chi)$, we obtain the system of equations as

$$\begin{bmatrix} 4 & -16 & 12 & -1 \\ -12 & -72 & -16 & 5 \\ 8 & 208 & -36 & -9 \\ 8 & 88 & 64 & 5 \\ -12 & -432 & 4 & 5 \\ 4 & 104 & 48 & -9 \\ 0 & 240 & 20 & 5 \\ 0 & -120 & 0 & -1 \end{bmatrix} \begin{bmatrix} u_f \\ lc^2 \\ \mu c \\ \frac{\sqrt{\Phi}}{2\alpha_1} \end{bmatrix} = \begin{bmatrix} 0 \\ 0 \\ 0 \\ 0 \\ 0 \\ 0 \\ 0 \\ 0 \end{bmatrix} \tag{A.11}$$

Again after some elementary matrix operations, we obtain the following system of equations,

$$\begin{aligned} 4u_f - 16lc^2 - 12\mu c - \alpha_1\sqrt{\Phi}_s &= 0, \\ -120lc^2 - \alpha_1\sqrt{\Phi}_s &= 0, \quad 20\mu c + 3\alpha_1\sqrt{\Phi}_s = 0. \end{aligned} \tag{A.12}$$

From these equations, we obtain

$$\sqrt{\Phi}_s = \frac{2u_f}{b\sqrt{\alpha}}, \quad c = \frac{\nu}{18\sqrt{\alpha}}. \tag{A.13}$$

These results are also well agree with our fixed point analysis of SB equation [Eq. (21)].

References

1. F.S. Mozer, C.W. Carlson, M.K. Hudson, R.B. Torbert, B. Parady, J. Yatteau, M.C. Kelley, Phys. Rev. Lett. **38**, 292 (1977)

2. C.A. Cattell, J. Dombek, J.R. Wygant, M.K. Hudson, F.S. Mozer, M.A. Temerin, W.K. Peterson, C.A. Kletzing, C.T. Russell, R.F. Pfaff, *Geophys. Res. Lett.* **26**, 425 (1999)
3. R.L. Tokar, S.P. Gary, *Geophys. Res. Lett.* **11**, 1180 (1984)
4. T. Miyake, Y. Omura, H. Matsumoto, *J. Geophys. Res.: Space Phys.* **105**, 23239 (2000)
5. R. Ergun, C. Carlson, L. Muschietti, I. Roth, J.P. McFadden, *Nonlinear Process. Geophys.* **6**, 187 (1999)
6. C. Cattell, J. Dombek, J. Wygant, J.F. Drake, M. Swisdak, M.L. Goldstein, W. Keith, A. Fazakerley, M. André, E. Lucek et al., *J. Geophys. Res.: Space Phys.* **110**, A01211 (2005)
7. S. Chowdhury, S. Biswas, N. Chakrabarti, R. Pal, *Phys. Plasmas* **24**, 062111 (2017)
8. B.D. Fried, R.W. Gould, *Phys. Fluids* **4**, 139 (1961)
9. M.F. Thomsen, H.C. Barr, S.P. Gary, W.C. Feldman, T.E. Cole, *J. Geophys. Res.: Space Phys.* **88**, 3035 (1983)
10. W.C. Feldman, R.C. Anderson, S.J. Bame, *J. Geophys. Res.: Space Phys.* **88**, 96 (1983)
11. S.P. Gary, R.L. Tokar, *Phys. Fluids* **28**, 2439 (1985)
12. N. Dubouloz, R. Pottelette, M. Malingre, R.A. Treumann, *Geophys. Res. Lett.* **18**, 155 (1991)
13. N. Dubouloz, R.A. Treumann, R. Pottelette, M. Malingre, *J. Geophys. Res.: Space Phys.* **98**, 17415 (1993)
14. C. Cattell, R. Bergmann, K. Sigsbee, C. Carlson, C. Chaston, R. Ergun, J. McFadden, F.S. Mozer, M. Temerin M, R. Strangeway et al., *Geophys. Res. Lett.* **25**, 2053 (1998)
15. D. Schriver, M.A. Abdalla, *Geophys. Res. Lett.* **16**, 899 (1989)
16. R.E. Ergun, C.W. Carlson, J.P. McFadden, F.S. Mozer, G.T. Delory, W. Peria, C.C. Chaston, M. Temerin, I. Roth, L. Muschietti et al., *Geophys. Res. Lett.* **25**, 2041 (1998)
17. J.R. Franz, P.M. Kintner, J.S. Pickett, *Geophys. Res. Lett.* **25**, 1277 (1998)
18. R. Pottelette, R.E. Ergun, R.A. Treumann, M. Berthomier, C.W. Carlson, J.P. McFadden, I. Roth, *Geophys. Res. Lett.* **26**, 2629 (1999)
19. R.L. Mace, S. Baboolal, R. Bharuthram, M.A. Hellberg, *J. Plasma Phys.* **45**, 323 (1991)
20. S.V. Singh, G.S. Lakhina, *Planet. Space Sci.* **49**, 107 (2001)
21. M. Berthomier, R. Pottelette, L. Muschietti, I. Roth, C.W. Carlson, *J. Geophys. Res.: Space Phys.* **30**, 1 (2003)
22. M. Dutta, S. Ghosh, N. Chakrabarti, *Phys. Rev. E* **86**, 066408 (2012)
23. A. Biswas, S. Ghosh, N. Chakrabarti, *Phys. Scr.* **95**, 105603 (2020)
24. M. Ghosh, S. Pramanik, S. Ghosh, *Phys. Lett. A* **396**, 127242 (2021)
25. J.R. Asbridge, S.J. Bame, I.B. Strong, *J. Geophys. Res.* **73**, 5777 (1968)
26. Y. Futaana, S. Machida, Y. Saito, A. Matsuoka, H. Hayakawa, *J. Geophys. Res.: Space Phys.* **108**, SMP-15-1 (2003)
27. R. Lundin, A. Zakharov, R. Pellinen, H. Borg, B. Hultqvist, N. Pissarenko, E.M. Dubinin, S.W. Barabash, I. Liede, H. Koskinen, *Nature* **341**, 609 (1989)
28. D. Henry, J.P. Trguier, *J. Plasma Phys.* **8**, 311 (1972)
29. A. Mamun, *Eur. Phys. J. D* **45**, 323 (2000)
30. T.S. Gill, P. Bala, H. Kaur, N.S. Saini, S. Bansal, J. Kaur, *Eur. Phys. J. D* **31**, 91 (2004)
31. A.P. Misra, A.R. Chowdhury, *Eur. Phys. J. D* **37**, 105 (2006)
32. D. Chakraborty, S. Ghosh, *Eur. Phys. J. D* **75**, 1 (2021)
33. H. Schamel, *Plasma Phys.* **14**, 905 (1972)
34. H. Schamel, *J. Plasma Phys.* **9**, 377 (1973)
35. H. Schamel, *Phys. Scr.* **20**, 306 (1979)
36. H. Schamel, *Phys. Scr.* **T2A**, 228 (1982)
37. H. Schamel and J. Korn, *Phys. Scr.* **T63**, 63 (1996)
38. W.F. El-Taibany, *J. Geophys. Res.: Space Phys.* **110**, 1 (2005)
39. S. Sultana, A. Mannan, R. Schlickeiser, *Eur. Phys. J. D* **73**, 220 (2019)
40. D.S. Montgomery, R.J. Focia, H.A. Rose, D.A. Russell, J.A. Cobble, J.C. Fernández, R.P. Johnson, *Phys. Rev. Lett.* **87**, 155001 (2001)
41. G. Petracconi, H.S. Maciel, *J. Phys. D: Appl. Phys.* **36**, 2798 (2003)
42. R.E. Ergun, Y.J. Su, L. Andersson, C.W. Carlson, J.P. McFadden, F.S. Mozer, D.L. Newman, M.V. Goldman, R.J. Strangeway, *Phys. Rev. Lett.* **87**, 045003 (2001)
43. L. Andersson, R.E. Ergun, D.L. Newman, J.P. McFadden, C.W. Carlson, Y.J. Su, *Phys. Plasmas* **9**, 3600 (2002)
44. R.E. Ergun, L. Andersson, D. Main, Y.J. Su, D.L. Newman, M.V. Goldman, C.W. Carlson, A.J. Hull, J.P. McFadden, F.S. Mozer, *J. Geophys. Res.: Space Phys.* **109**, 1 (2004)
45. N.B. Nagel, *Phys. Chem. Earth, Part A: Solid Earth Geod.* **26**, 3 (2001)
46. A.V. Volosevich, Y.I. Galperin, *Ann. Geophys.* **15**, 890 (1997)
47. S. Watanabe, *J. Phys. Soc. Jpn.* **45**, 276 (1978)
48. A. Adak, S. Sengupta, *Eur. Phys. J. D* **73**, 197 (2019)
49. J.K. Xue, *Eur. Phys. J. D* **26**, 211 (2003)
50. S. Sultana, I. Kourakis, *Eur. Phys. J. D* **66**, 100 (2012)
51. O. Pezzia, F. Valentini, P. Veltri, *Eur. Phys. J. D* **68**, 128 (2014)
52. A.R. Seadawy, I. Mujahid, L. Dianchen, *Phys. A: Stat. Mech. Appl.* **544**, 123560 (2020)
53. W. Malfliet, W. Hereman, *Phys. Scr.* **54**, 563 (1996)
54. R.C. Davidson, *Methods in Nonlinear Plasma Theory* (Academic, New York, 1972)
55. T. Taniuti, *Prog. Theor. Phys. Suppl.* **55**, 1 (1974)
56. V.I. Karpman, *Phys. Scr.* **20**, 462 (1979)
57. V.Y. Belashov, S.V. Vladimirov, *Solitary Waves in Dispersive Complex Media* (Springer, Berlin, 2005)
58. V.I. Karpman, *Non-linear Waves in Dispersive Media: International Series of Monographs in Natural Philosophy*, vol. 71 (Elsevier, Amsterdam, 2016)
59. H. Schamel, J. Korn, *Phys. Scr.* **T63**, 63 (1996)
60. R.S. Johnson, *J. Fluid Mech.* **42**, 49 (1970)

Springer Nature or its licensor (e.g. a society or other partner) holds exclusive rights to this article under a publishing agreement with the author(s) or other rightsholder(s); author self-archiving of the accepted manuscript version of this article is solely governed by the terms of such publishing agreement and applicable law.